Arch. Metall. Mater. **64** (2019), 2, 551-557

DOI: 10.24425/amm.2019.127577

CHEENEPALLI NAGARJUNA*, BABU MADAVALI*, MYEONG-WON LEE*,
SUK-MIN YOON*, SOON-JIK HONG*#

REDUCTION OF THERMAL CONDUCTIVITY THROUGH THE DISPERSION OF TiC NANOPARTICLES INTO A P-TYPE $Bi_{0.5}Sb_{1.5}Te_3$ ALLOY BY BALL MILLING AND SPARK PLASMA SINTERING

The dispersion of nanoparticles in the host matrix is a novel approach to enhance the thermoelectric performance. In this work, we incorporate the TiC (x = 0, 1 and 2 wt.%) nanoparticles into a p-type $Bi_{0.5}Sb_{1.5}Te_3$ matrix, and their effects on microstructure and thermoelectric properties were systematically investigated. The existence of TiC contents in a base matrix was confirmed by energy dispersive X-ray spectroscopy analysis. The grain size decreases with increasing the addition of TiC content due to grain boundary hardening where the dispersed nanoparticles acted as pinning points in the entire matrix. The electrical conductivity significantly decreased and the Seebeck coefficient was slightly enhanced, which attributes to the decrease in carrier concentration by the addition of TiC content. Meanwhile, the lowest thermal conductivity of 0.97 W/mK for the 2 wt.% TiC nanocomposite sample, which is ~16% lower than 0 wt.% TiC sample. The maximum figure of merit of 0.90 was obtained at 350 K for the 0 wt.% TiC sample due to high electrical conductivity. Moreover, the Vickers hardness was improved with increase the addition of TiC contents.

Keywords: $Bi_{0.5}Sb_{1.5}Te_3$ alloys; Nanocomposites; Ball milling; Spark plasma sintering; Thermoelectric properties

1. Introduction

Since the last few decades, the continuous developments in worldwide industrial and automobile engineering technology lead to create a demand of energy sources and climate change by the combustion of fossil fuels, which are the most extensive problems had been facing by the humankind [1]. For this, an alternative green thermoelectric (TE) energy conversion system with zero emission of CO_2 gases have been acquired a considerable attention for harvesting the waste heat energy from the exhausted heat sources [2]. The conversion efficiency of a thermoelectric material can be evaluated by a dimensionless quantity named as figure of merit, $ZT = (\alpha^2\sigma/\kappa)T$, where α, σ, κ, and T are the Seebeck coefficient, electrical conductivity, thermal conductivity and absolute temperature of the material respectively [3]. The highest ZT value suggesting that TE material having a greater conversion efficiency, thus for achieving high ZT, the material should be a high power factor value ($\alpha^2\sigma$), while the low thermal conductivity (κ) are required. However, such requirements are difficult to be satisfied in case of bulk thermoelectric materials rather than nanocomposites, due to having strong dependency behavior on carrier concentration [4]. In the recent years, numerous studies have been employed to develope the high-performance TE materials by adopting the nanostructuring methods [5-8].

Due to having an excellent thermoelectric performance and reliability, Bi_2Te_3 based materials are the most desirable candidates near the room temperature applications such as power generation and refrigeration [9]. Usually, the polycrystalline Bi_2Te_3 based bulk materials can give less thermal conductivity than single crystalline materials because having the more density of grain boundaries [10]. Further reduce the thermal conductivity in bulk materials for achieving high ZT, the nanostructuring or nanocomposite (embedding nanoparticles in base alloys) approach was implemented recently. Such type of approaches would really assist to enhance the low frequency of carrier/phonon scattering at grain boundaries, which resulting in the reduction of thermal conductivity was observed in bulk TE materials [11]. Previously, many comprehensive studies have undergone to understanding the influence of nanoinclusions in bulk materials through various manufacturing processes and its impact on transport properties of TE materials [12,13]. Cao et al. reported that the highest ZT of 1.47 for p-type Bi_2Te_3/Sb_2Te_3 bulk nanocomposites with laminated structures fabricated by the hydrothermal and hot-pressing process [14]. Kim et al. reported a maximum ZT of 1.5 at 323 K by incorporating the 0.3 Vol.% of Al_2O_3 nanoparticles into a $Bi_{0.5}Sb_{1.5}Te_3$ matrix by ball milling process. Especially, the obtained ZT is due to the enhancement of power factor and the reduction in thermal conductivity [15]. On the other hand, dispersion of ceramic

* KONGJU NATIONAL UNIVERSITY, DIVISION OF ADVANCED MATERIALS ENGINEERING, CHEONAN-SI 31080, REPUBLIC OF KOREA

Corresponding author: hongsj@kongju.ac.kr

nanoparticles into bulk materials, also an effective approach to reinforce the TE properties. Recent reports have shown that most of the significant improvements of *ZT* have been achieved by the enhancement of Seebeck coefficient through energy carrier filtering effect. Meanwhile, 45%, and 36% enhancement in Seebeck coefficient was achived by dispersing the 2wt.% Y_2O_3 and 4wt.% ZrO_2 ceramic nanoparticles in a p-type $Bi_{0.5}Sb_{1.5}Te_3$ alloy respectively. In addition, the thermal conductivity was strongly decreased due to the enhancement of carrier or phonon scattering at the newly formed interfaces [16,17]. In our report, we introduced the TiC nanoparticles in a p-type $Bi_{0.5}Sb_{1.5}Te_3$ alloy through a high energy ball milling process to make the nanocomposites. And we expected that dispersed nanoparticles would effectively suppress the thermal conductivity by intensifying the interface scattering, which leads to enhance the figure of merit.

In this report, we fabricated the p-type $Bi_{0.5}Sb_{1.5}Te_3/x$-TiC (x = 0, 1 and 2 wt.%) nanocomposites by ball milling and spark plasma sintering respectively. We investigated the effects of TiC dispersion on thermoelectric properties as a function of temperature. The phase and morphological studies have been conducted to observe the TiC contents and it displays that the addition of TiC contents would effectively decrease the grain size. As a result, the electrical conductivity drastically decreases and the Seebeck coefficient was slightly enhanced. In addition, the thermal conductivity was significantly decreased by ~16% as compared to the 0 wt.% TiC sample.

2. Experimental procedure

High purity elemental chunks of bismuth (Bi, 99.999%), antimony (Sb, 99.999%), tellurium (Te, 99.999%) and titanium carbide nanoparticles (TiC, 99%, 40-50 nm) were used as starting materials for the following study. In order to prepare the required composition of p-type $Bi_{0.5}Sb_{1.5}Te_3$ alloy, (Here onwards referred as BiSbTe) the raw elements were weighed according to the stoichiometric ratio. The gas atomization (GA) process was used for the fabrication of alloy powders and the processing conditions were described in our previous report [4]. We utilized the high energy ball milling process to disperse the TiC nanoparticles into the BiSbTe base matrix. The alloy powder and with different TiC (x = 0, 1 and 2 wt.%) contents were loaded into a zirconia jars and balls with the weight ratio of ball to powder were taken as 15:1 for 20 min with a rotating speed of 800 rpm. The obtained composite powders were heat-treated at 470°C before the sintering process in a vacuum condition, to remove the moisture content in an alloy powder. Subsequently, the heat-treated powders were consolidated by spark plasma sintering (SPS) at 400°C for 10 min in a vacuum by applying an axial pressure of 50 MPa. The crystal structure of composite powder and bulk samples were analyzed by X-ray diffraction technique (Rigaku, Miniflex-600 diffractometer using CuK_α radiation). The powder morphology and fractured surface of bulk samples were investigated using the scanning electron microscopy (SEM-MIRA LMH II TESKAN, Czech republic). And the existence of TiC nanoparticles in the base matrix was confirmed by SEM equipped with energy dispersive x-ray spectroscopy (EDS) analysis. The relative density (d) and Vickers hardness tests were carried out to examine the mechanical stability of the bulk samples by Archimedes principle and micro Vickers indenter measurement system respectively. The thermoelectric properties including electrical conductivity, Seebeck coefficient and power factor were measured by thermoelectric power factor measurement system (TEPF-800). Thermal diffusivity (λ) was measured by a laser flash method (Netzsch LFA 467) and the specific heat (C_p) was calculated with the Perkin Elmer DSC-8000. Thermal conductivity (κ) was determined from the measured λ, C_p and d by substituting in the relation $\kappa = \lambda.C_p.d$. Finally, we calculated the dimensionless figure of merit using the calculated power factor and thermal conductivity at each temperature.

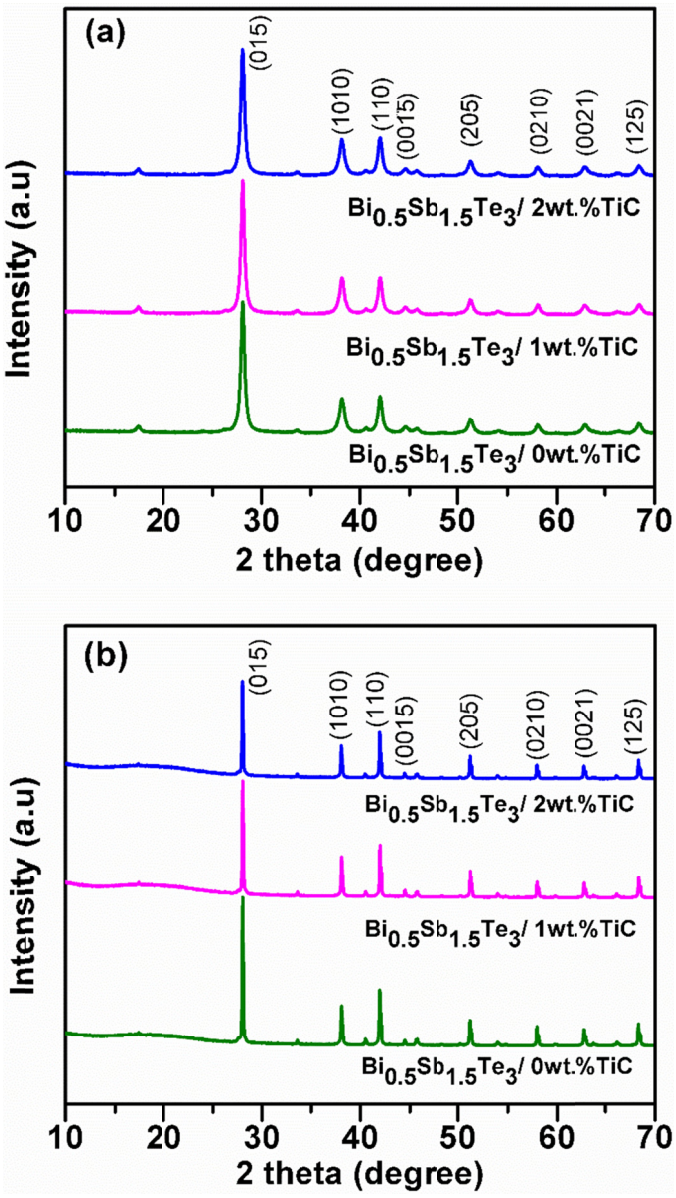

Fig. 1. X-ray diffraction patterns of the p-type BiSbTe/x-TiC (x = 0, 1 and 2wt.%) nanocomposite (a) powder and (b) bulk samples

3. Results and discussion

The X-ray diffraction patterns of the p-type BiSbTe/*x*-TiC (x = 0, 1 and 2 wt.%) nanocomposite powder and bulk samples were shown in Fig. 1 (a) and (b) respectively. All the diffraction peaks are related to the ternary alloy of $Bi_{0.5}Sb_{1.5}Te_3$ composites and there are no distinct peaks of TiC was detected by XRD in the nanocomposite samples because the addition of TiC contents are too low. The indexed peaks of all the composite samples are identified as single phase along the rhombohedral crystal structure with space group $R\bar{3}m$. On the other hand, the indexed peaks are good agreement with the standard diffraction data (JCPDS # 49-1713). The bulk samples show a sharper peak compared to the as-milled composites, it reveals that the crystallinity has improved after the spark plasma sintering.

Fig. 2 represents the SEM micrographs of the TiC nanoparticles and BiSbTe/*x*-TiC (x = 0, 1 and 2 wt.%) nanocomposite powders. As can be seen from the Fig. 2(a), the TiC nanoparticles are agglomerated and some of the particles are spherical in shape with a diameter of about 40-50 nm. The TiC nanoparticles were dispersed in a BiSbTe matrix by using the high energy ball milling process to make the nanocomposites. The powder morphology of BiSbTe/*x*-TiC (x = 0, 1 and 2 wt.%) nanocomposite powders can be seen in Fig. 2(b), (c) and (d) respectively. It is observed that all the composite powders were in irregular shape and the estimated average size is about ~2 μm. Moreover, the addition of 1 and 2 wt.% TiC nanocomposites show a decrease in particle size along with agglomeration compared to that of 0 wt.% TiC nanocomposite powder.

Fig. 3 shows the SEM micrographs of the fractured surface of BiSbTe/*x*-TiC with (a) x = 0, (b) x =1 and (c) x = 2 wt.% nanocomposite bulk samples, which were fabricated by the spark plasma sintering. Fig. 3(a) shows the randomly oriented large grains and having smooth surface was observed in the 0 wt.% TiC sample. The average grain size is estimated about below ~10 μm. It is evident from the Fig. 3(b) and 3(c), grain size was gradually decreased upon the dispersion of TiC (1 and 2 wt.%) content, because the dispersed nanoparticles acted as pinning points throughout the matrix and it would prevents the grain growth while the sintering process. We believe that this type of decreased grain sizes would enhance the carrier or phonon scattering at the surface of grain boundaries, resulting to decrease the thermal conductivity and enhances the performance of a material. Fig. 3(d) shows the elemental mapping analysis for the 2 wt.% TiC sample corresponding to the fracture surface of Fig. 3(c). The obtained results reveal that all the base elements are well matched with the nominal composition and the dispersed TiC nanoparticles were also detected by the EDS analysis.

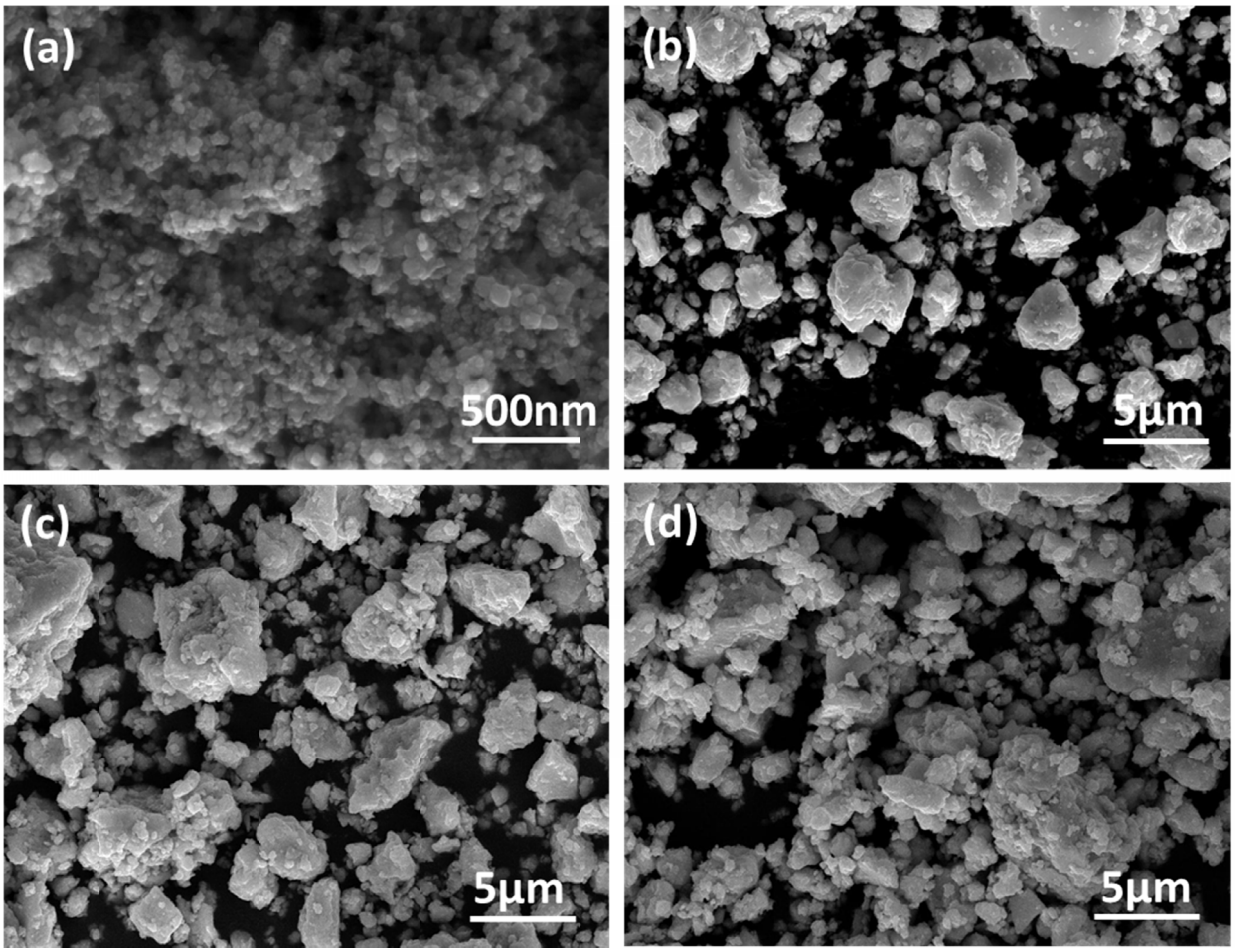

Fig. 2. Powder morphology of (a) TiC nanoparticles, (b) BiSbTe/0wt.% TiC, (c) BiSbTe/1wt.% TiC and (d) BiSbTe/2wt.% TiC nanocomposite powders

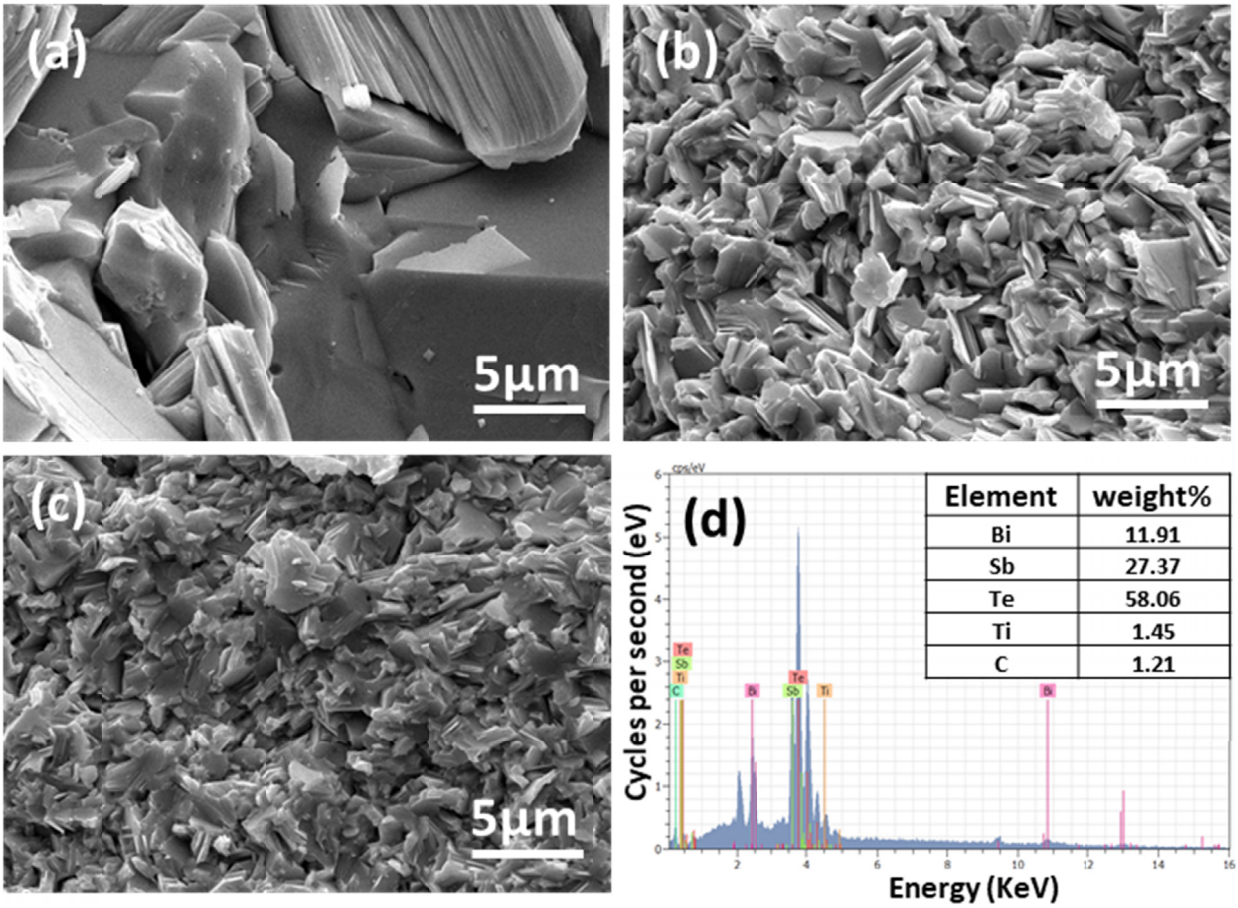

Fig. 3. Fracture surface of (a) BiSbTe/0 wt.% TiC, (b) BiSbTe/1wt.% TiC and (c) BiSbTe/2wt.% TiC nanocomposite bulk samples and (d) EDS mapping analysis for the BiSbTe/2wt% TiC nanocomposite sample

The temperature dependence of transport properties of the electrical conductivity, Seebeck coefficient and power factors of the BiSbTe/x-TiC (x = 0, 1 and 2 wt.%) nanocomposite samples were illustrated in Fig. 4(a), (b) and (c) respectively. The electrical conductivity (σ) of all the samples decreased as a function of increasing the temperature and it suggested that all the samples exhibited a degenerate semiconductor or metal like behaviour [18]. Furthermore, the electrical conductivity decreases with increase of TiC content. The maximum σ was observed to be ~610 $\Omega^{-1}cm^{-1}$ for the 0 wt.% TiC sample and it is drastically decreased by the addition TiC (1 and 2 wt.%) content. Generally, the electrical conductivity can be determined from the density of charge carriers (n_c) and carrier mobility (μ) and its typical relation can be expressed by the following equation.

$$\sigma = n_c.e.\mu \qquad (1)$$

Where, n_c is the number of charge carriers would be active in the conduction process, e is the carrier charge and μ is the mobility of the charge carriers. To study the influence of TiC contents on transport properties, we investigated the carrier concentration and mobility at room temperature and it can be seen in Table 1. The results reveal that the significant reduction of electrical conductivity was achieved by the decrease in carrier concentration and mobility with the addition of TiC content. The decrease of carrier concentration might be due to the mismatch of band alignment between the host matrix and incorporated nanoparticles [16]. Besides, the dispersed nanoparticles would form inside the grains or around the grain boundaries and it causes to enhance the carrier scattering at the interfaces, resulting to the decrease in carrier mobility. And the similar behavior was observed in previous reports [16,17].

Fig. 4(b) shows the temperature dependence of the Seebeck coefficient of p-type BiSbTe/x-TiC (x = 0, 1 and 2 wt.%) nanocomposite bulk samples. All the samples exhibited p-type conducting behavior, and it is suggesting that predominant charge

TABLE 1

The physical properties of p-type BiSbTe/x-TiC (x = 0, 1 and 2wt.%) nanocomposite bulk samples were measured at room temperature

Sample	Rel. density (%)	Hardness (Hv)	n_c (10^{19}/cm^3)	μ_h (10^2cm^2/Vs)	L_0 (10^{-8} WΩK^{-2})
BiSbTe/0wt.% TiC	97.01	114	1.47	2.58	1.6328
BiSbTe/1wt.% TiC	96.54	130	1.23	2.26	1.6200
BiSbTe/2wt.% TiC	96.03	143	1.19	2.21	1.6186

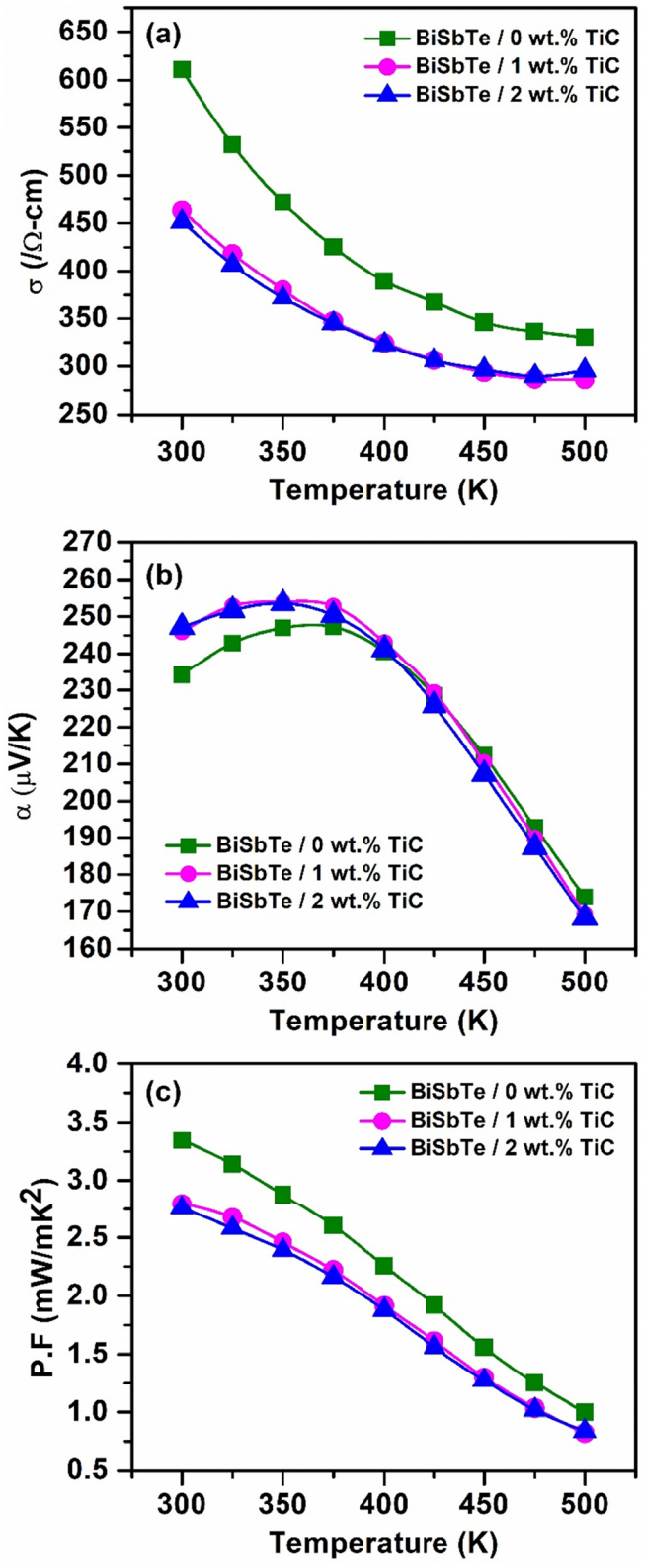

Fig. 4. Temperature dependence of (a) electrical conductivity (b) Seebeck coefficient and (c) power factor of p-type BiSbTe/*x*-TiC (x = 0, 1 and 2wt.%) nanocomposite samples

carriers are holes in the entire measuring temperature. Firstly, the Seebeck coefficient of all the samples is somewhat increased up to 350 K after that gradually decreases with an increasing temperature. The decrease of Seebeck coefficient may be due to the excitation of minority carrier conduction at elevated temperatures [19]. It is known that the relationship between the Seebeck coefficient and carrier concentration can be determined from the following equation.

$$S = \frac{8\pi^2 K_B^2}{3eh^2} m^* T \left(\frac{\pi}{3n}\right)^{2/3} \quad (2)$$

Where K_B, e, h, m^*, n is the Boltzmann constant, carrier charge, Plank's constant, effective mass of carriers and density of charge carriers respectively. The Seebeck coefficient was slightly enhanced for the addition of TiC contents from 0 to 2 wt.%. which is attributed to the obivious decrease in carrier concentration values (shown in Table. 1). At room temperature, the maximum Seebeck coefficient of 247 μV/K was observed for the 2 wt.% TiC sample, which is comparatively higher than 0 wt.% of TiC sample.

Fig. 4(c) shows the temperature dependence of power factor ($S^2\sigma$) values of all the nanocomposite samples and which can be determined from the measured electrical conductivity and Seebeck coefficient values. The power factors of all the samples decrease with increasing temperature due to decreasing behaviour of electrical conductivity, it can be seen in Fig. 4(a). The maximum power factor of 3.34 mW/mK^2 was obtained at 300 K for the 0 wt.% TiC sample. Meanwhile, we found the decreased power factor values with increasing the addition of TiC content from 0 to 2 wt.% throughout the measuring temperature.

The temperature dependence of total thermal conductivity (κ) of the BiSbTe/*x*-TiC (x = 0, 1 and 2 wt.%) nanocomposite samples and the variation as a function of temperature can be seen in Fig. 5(a). The thermal conductivity of all the samples increases with increasing the operating temperature, at the same time we found the gradual decrease of thermal conductivity with the addition of TiC content from 0 to 2 wt.%. At room temperature the total thermal conductivity of 1.13 W/mK was observed for the 0 wt.% TiC sample and it decreased to 0.97 W/mK for the 2 wt.% TiC sample, which is ~16% lower than that of 0 wt.% TiC sample. Generally, the total thermal conductivity is contributed by two main processes via charge carriers through the crystal lattice and phonons through the lattice vibrations. In order to examine the electronic contribution to the total thermal conductivity, we have to determine the Lorenz number and it can be calculated from the following expression [20].

$$L = 1.5 + \exp\left[-\frac{|s|}{116}\right] \quad (3)$$

Where L is the Lorentz number (L = 2.45×10^{-8} WΩK^{-2} for degenerate semiconductors) and S is the Seebeck coefficient (μv/K). Based on Wiedemann Franz law ($\kappa_e = L\sigma T$), we computed the electronic thermal conductivity and presented in Fig. 5 (b). Firstly, the electronic thermal conductivity was slighltly decreases and then increases at higher temperature, caused to the bipolar conduction [21]. Besides, the electronic thermal conductivity was significantly decreased with increase the addition of TiC content when compared with the 0 wt.% TiC sample. This behaviour was mainly attributed to the decrease of electrical conductivity with increase the addition of TiC

content. The lattice thermal conductivity (κ_l) can be calculated by the subtraction of electronic component (κ_e) from the total thermal conductivity (κ). Fig. 5(c) shows the decreased lattice thermal conductivity with increase the addition of TiC content, due to the dispersed nanoparticles would form more density of grain boundaries, resulting to the intensified phonon scattering at newly formed interfaces. From this results we concluded that the significant reduction of total thermal conductivity by the greater amount of decrease in electronic thermal conductivity rather than lattice thermal conductivity.

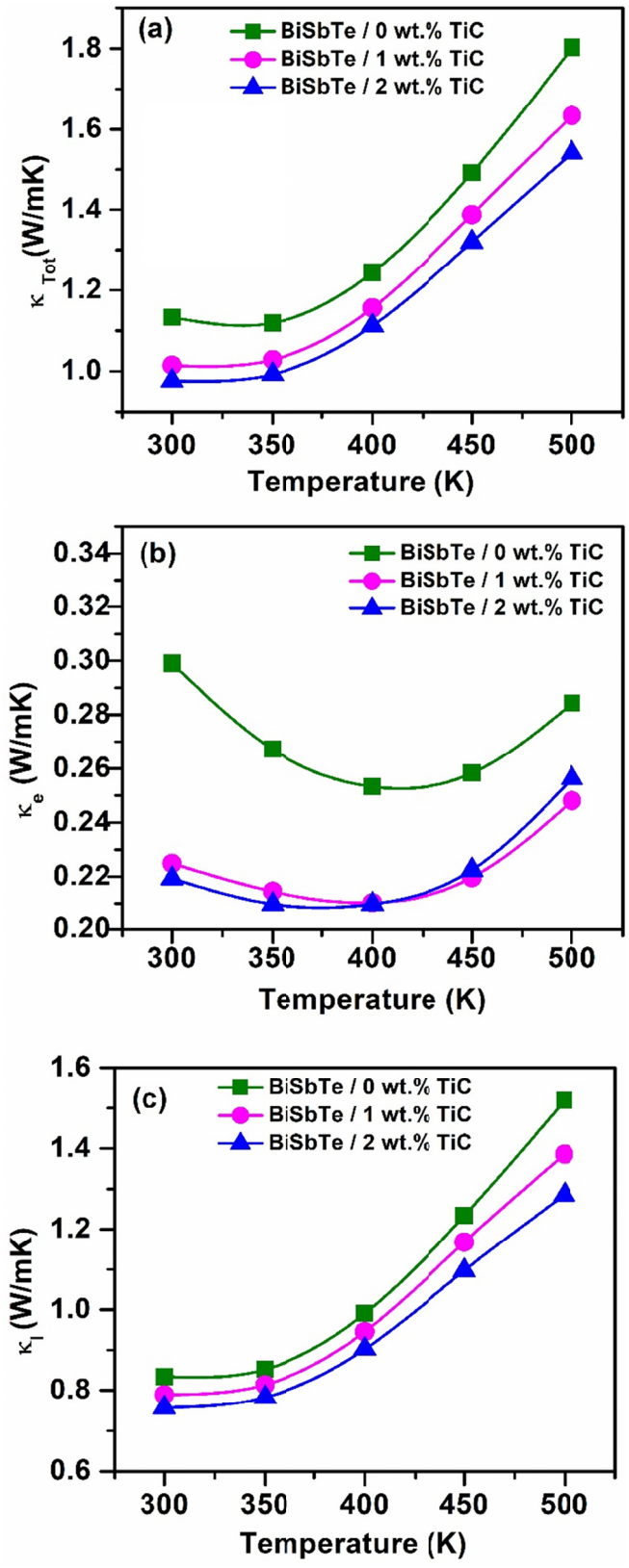

Fig. 5. Temperature dependence of (a) thermal conductivity (b) electronic thermal conductivity (κ_e) and (c) lattice thermal conductivity (κ_l) of BiSbTe/x-TiC (x = 0, 1 and 2wt.%) nanocomposite samples

The temperature dependence of the dimensionless figure of merit (ZT) for all the nanocomposite samples was plotted in Fig. 6. The ZT values were decreased with increasing the temperature. It is mainly due to the decrease in power factors of all the nanocomposite samples. At the same time we found a little lower ZT values for the 1 and 2 wt.% of TiC samples than 0 wt.% TiC sample. The maximum ZT of 0.90 was achieved at 350 K for the 0 wt.% TiC sample, which is caused by having higher electrical conductivity other than TiC (1 and 2 wt.%) consisted of bulk samples. The obtained ZT results are approximately similar with the previously reported $Bi_{0.5}Sb_{1.5}Te_3$/ZnO composites [22].

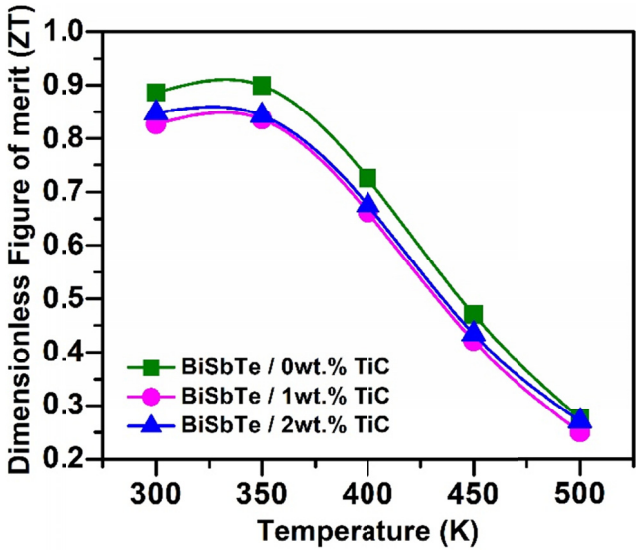

Fig. 6. The temperature dependence of dimensionless figure of merit for the p-type BiSbTe/x-TiC (x = 0, 1 and 2 wt.%) nanocomposite samples measured as a function of temperature

Table. 1 shows the relative density and hardness of the bulk samples and it can be measured at room temperature. The relative density of all the samples show over than 96%, however, it is slightly decreases with increasing the addition of TiC content from 0-2 wt.%, because the dispersed nanoparticles would apply backstress during the sintering process [22]. Besides, the Vickers hardness of the bulk samples gradually increases with an increase the addition of TiC content, due to the dispersed nanoparticles would enhance the grain boundary strengthening or hardening behavior.

4. Conclusion

In summary, we have successfully fabricated the p-type BiSbTe/x-TiC (x = 0, 1 and 2 wt.%) nanocomposites by the combination of high energy ball milling and spark plasma sinter-

ing techniques. And we studied the thermoelectric properties by varying the TiC contents as a function of temperature ranging from 300-500 K. With increasing TiC content, the electrical conductivity was significantly decreased while the Seebeck coefficient was slightly enhanced due to decrease in carrier concentration. Meanwhile, the thermal conductivity was significantly decreased by ~16% than the 0 wt.% TiC sample, which is due to the significant decrease in electronic contribution to the total thermal conductivity. The maximum figure of merit *ZT* of 0.90 was achieved at 350 K for the 0 wt.% TiC sample due to higher electrical conductivity than other samples.

Acknowledgement

This work was supported by the Industrial Strategic Technology Development Program-Development of high efficient thermoelectric module with figure of merit (Z) 3.4 ($X10^{-3}$) by using 1.0 kg/batch scale productible polycrystalline thermoelectric material with average figure of merit (ZT) 1.4 and over (10063286) funded By the Ministry of Trade, Industry & Energy (MOTIE, Korea).

REFERENCES

[1] G.J. Snyder, E.S. Toberer, Nat. Mater. **7**, 105-114 (2008).

[2] H.S. Kim, P. Dharmaiah, B. Madavali, R. Ott, K.H. Lee, S.J. Hong, Acta. Mat. **128**, 43-53 (2017).

[3] S.M. Yoon, C. Nagarjuna, D.W. Shin, C.H. Lee, M. Babu, S.J. Hong, K.H. Lee, J. Korean Powder Metall. Inst. **24**, 357-363 (2017).

[4] B. Madavali, H.S. Kim, K.H. Lee, Y. Isoda, F. Gascoin, S.J. Hong, Mater Des. **112**, 485-494 (2016).

[5] W.H. Shin, K. Ahn, M. Jeong, J.S. Yoon, J.M. Song, S. Lee, W.S. Seo, Y.S. Lim, J. Alloy. Compd. **718**, 342-348 (2017).

[6] Y. Lan, A.J. Minich, G. Chen, Z.F. Ren, Adv Funct Mater. **20**, 357 (2010).

[7] A.J. Minnich, M.S. Dresselhaus, Z.F. Ren, G. Chen, Energy Environ. Sci. **2**, 466-479 (2009).

[8] C.J. Vineis, A. Shakouri, A. Majumdar, M.G. Kanatzidis, Adv. Mater. **22**, 3980 (2010).

[9] W. Xie, J. He, H.J. Kang, X. Tang, S. Zhu, M. Laver, S. Wang, J.R.D. Copley, C M. Brown, Q. Zhang, T.M. Tritt, Nano Lett. **10**, 3283-3289 (2010).

[10] S. Grasso, N. Tsujii, Q. Jiang, J. Khaliq, S. Maruyama, M. Miranda, K. Simpson, T. Mori, M.J. Reece, J. Mater. Chem. C, **1**, 2362-2367 (2013).

[11] G.B. Granger, A. Addad, C. Navone, M. Soulier, J. Simon, P.D. Szkutnik, Acta Mater. **60**, 4523-4530 (2012).

[12] B. Liu, J. Hu, J. Zhou, R. Yang, Materials. **10**, 418 (2017).

[13] S.V. Faleev, F. Leonard, Phys. Rev. B. **77** (21), 214304 (2008).

[14] Y.Q. Cao, X.B. Zhao, T.J. Zhu, X.B. Zhang, J.P. Tu, Appl. Phys. Lett. **92**, 143106 (2008).

[15] K.T. Kim, G.H. Ha, J. Nano Mat. doi.org/10.1155/2013/821657 (2013).

[16] B. Madavali, H.S. Kim, K.H. Lee, S.J. Hong, Intermetallics. **82**, 68-75 (2017).

[17] B. Madavali, H.S. Kim, K.H. Lee, S.J. Hong, J. Appl. Phys. **121**, 225104 (2017).

[18] B. Poudel, Q. Hao, Y. Ma, Y. Lan, A. Minnich, B. Yu, X. Yan, D. Wang, A. Muto, D. Vashaee, X. Chen, J. Liu, M.S. Dresselhaus, G. Chen, Z. Ren, Science. **320**, 634-638 (2008).

[19] J.H. Bahk, A. Shakouri, Phys. Rev. B. **93**, 165209 (2016).

[20] H.S. Kim, Z.M. Gibbs, Y. Tang, H. Wang, G.J. Snyder, APL Mater. **3**, 041506 (2015).

[21] E.B. Kim, P. Dharmaiah, D. Shin, K.H. Lee, S.J. Hong, J. Alloy. Compd. **703**, 614-623 (2017).

[22] B. Madavali, C.H. Lee, H.S. Kim, K.H. Lee, S.J. Hong, Int. J. Appl. Ceram. Technol. **15**, 125-131 (2018).